J Mater Sci (2006) 41:6228–6236
DOI 10.1007/s10853-006-0318-y

Thermal expansion behaviour of ultra-high modulus carbon fibre reinforced magnesium composite during thermal cycling

M. Russell-Stevens · R. I. Todd · M. Papakyriacou

Received: 12 January 2005 / Accepted: 31 October 2005 / Published online: 2 September 2006

Abstract The thermally induced strain response of unidirectional P100S/AZ91D carbon fibre-reinforced magnesium composite was studied over five cycles in the ±100 °C temperature range. A temperature-dependent one-dimensional model was employed to predict the anticipated response to the cycling thermal environment. Strain hysteresis was observed during cycling and attributed to matrix yielding. First cycle residual plastic strains were modelled with reasonable agreement. Experimental results deviated from predictions during subsequent cycles with continued thermal ratcheting shifting the hysteresis loops to higher strains with increasing cycles. This was thought to be associated with interfacial debonding and frictional sliding at fibre/matrix interfaces. The effect of thermal treatment on composite expansion behaviour was investigated and the results discussed in terms of minimising thermally induced deformations during anticipated service conditions. Treatments were found to affect the first cycle behaviour, reducing in particular residual plastic strain generation. Matrix yield strength was exceeded over the thermal cycle due to a lack of sufficient hardening, and since interfacial conditions were unaltered, interfacial sliding and thermal ratcheting could not be eliminated. The potential for improvement of C/Mg composite thermal strain response was explored in the light of the current findings.

M. Russell-Stevens (✉) · R. I. Todd
Department of Materials, University of Oxford, Parks Road, Oxford OX1 3PH, England
e-mail: mark.russell-stevens@lmco.com

M. Papakyriacou
ARC Leichtmetall-Kompetenzzentrum Ranshofen GmbH, AMAG-FVA-Gebäude, Postfach 26, A-5282 Ranshofen, Oberösterreich, Austria

Introduction

Carbon fibre-reinforced magnesium composites (C/Mg) are candidate materials for space structures requiring high dimensional accuracy due to their high specific stiffness and low coefficient of thermal expansion (CTE) [1]. In comparison to conventional organic matrix composites, metal matrix composites (MMC) offer increased performance in terms of thermal and electrical conductivity, freedom from moisture effects [2], resistance to atomic oxygen degradation, and out-gassing [3].

Perhaps the most challenging aspect of the space environment, and the one which presents a significant problem for composites, is the transient thermal conditions experienced as a satellite in a low-earth orbit passes in and out of solar illumination; this can cause periodical temperature fluctuations between –100 °C and 100 °C.

Incorporating ultra-high modulus (UHM) carbon fibres, with a negative CTE (~–1.5 × 10^{-6} °C^{-1}) in the longitudinal direction in a magnesium matrix, with a large positive CTE (~27 × 10^{-6} °C^{-1}) can result in the generation of large thermal residual stresses with only modest temperature variations [2, 4, 5]. Thermal cycling studies of unidirectional (UD) C/Mg have shown strain hysteresis between heating and cooling segments of the cycle [4] and residual plastic strains (thermal strain ratcheting) [6], which were later shown to decrease in magnitude with increasing number of thermal cycles [7]. This complex and microstructurally-influenced thermal expansion behaviour, resulted in instantaneous and cumulative dimensional instability [4], especially at low temperatures [2].

In a classic study by Wolff et al. [4], numerical predictions confirmed the presence of hysteresis loops owing to matrix plasticity, during which the matrix does not contribute to the composite CTE [4]. Strain accumulation

was suggested to occur because of creep in the matrix but it was noted that further research in this matter was required [4, 6]. Although the study was made over a ±100 °C temperature range, accompanying experimental results were not consistent with this range and heating and cooling segments were varied between cycles. Furthermore, newly developed models can incorporate temperature dependence in the analysis [8] a factor not considered in the existing published works.

High precision space systems ideally require zero CTE. In the absence of this for practical systems, a linear and non-hysteretic thermal strain response is desired. Attempts have been made to eliminate thermal strain non-linearity and plastic strain generation through thermal processing to increases the elastic limit of the matrix to avoid plastic yield over the temperature cycle. For a fixed matrix composition—a necessary requirement to maintain interfacial bond conditions—techniques such as cryogenic conditioning [2, 5, 9–13], precipitation hardening and control of processing conditions [5], such as cooling rate, can be applied. A linear thermal expansion behaviour could not be achieved in thermally processed P100/AZ91C and QH21A C/Mg composites [11] with hysteresis reportedly remaining unaltered even after thermal cycling. However, details of the applied thermal treatments were omitted by the author. Other experiments have reported the treatment of C/Mg to –196 °C prior to thermal cycling [2, 12] have no marked effect apparent on the thermal strain behaviour. In neither case, however, is a comparison to untreated composites given.

Despite several studies there exists a paucity of careful experimental validation of thermal strain response of UHM C/Mg composites and on the effect of heat-treatment and cryogenic conditioning in controlling expansion behaviour. Accordingly the aim of this work is firstly, to revisit the thermal strain behaviour of UHM C/Mg by investigating two different volume fractions (V_f) of P100S/AZ91D and to measure experimentally the effect of a ±100 °C thermal cycle; secondly, to employ simple temperature-dependent models to determine whether the thermal response of composites can be predicted; and finally, to examine the effect of heat-treatment and matrix preconditioning via cryogenic cooling on composite thermal response and to assess the viability of modelling the thermal expansion behaviour of treated C/Mg MMCs.

Experimental procedure

The composites used in this investigation were fabricated by a filament winding and gas pressure infiltration casting technique at the Leichtmetall-Kompetenzzentrum Ranshofen, Austria. UHM carbon fibres of the type Thornel P100S were employed as the UD reinforcement in a matrix of AZ91D (Mg: 9 wt.% Al: 1 wt.% Zn: 0.2 wt.% Mn). Target fibre volume fractions were nominally ~50% and 60% as these represent the V_f values required for zero CTE in the longitudinal direction (based on ROM predictions) and the upper reinforcement value for this processing technique, respectively.

Material was tested in the as-cast (AC) state; T6 heat-treated (T6); and in the T6 condition followed by a cryogenic pre-conditioning treatment (T6-Cryo). In this work T6 heat treatment corresponds to a solution heat treatment of 12 h at 410 °C followed by an air cool to ambient, then subsequent artificial ageing at 200 °C for 15 h [14]. Pre-conditioning refers to a cryogenic cooling treatment to –196 °C for 5 min [13]. All specimens were encapsulated in silica tubes under a vacuum of 10^{-5} Pa or better prior to these treatments to prevent oxidation of the magnesium which is extreme at elevated temperatures.

The temperature-dependent yield strength of unreinforced AZ91D was determined through uniaxial tensile testing of specimens with a cylindrical reduced gauge length of 40 mm and a cross-sectional area of 28.3 mm^2. Samples were produced by gas pressure infiltrating empty carbon moulds under the same conditions as used for composite manufacture. Tests were performed between –100 °C and 250 °C on a 100 kN Zwick Z100 universal testing machine using automatic strain rates according to BS EN 10002.

The thermal strain response of the composite was measured in a Linseis Dilatometer equipped with a silica holder and at a heating and cooling rate of 2 °C/min. Specimen dimensions were 25 × 6 × 2 mm and end faces were polished, to a finish of 0.25 μm, flat, parallel and perpendicular to the length direction prior to testing. UD composites were tested in the longitudinal direction. The dilatometer was calibrated using a 25 mm NIST Standard Reference Material 739 fused silica rod over the ±100 °C temperature range. Dilatometer reproducibility error was determined to be approximately ±300 nm or 24 με based on the initial sample dimensions. Errors in CTE were determined from 12 measurements on a fused silica sample: an error of $\pm 0.07 \times 10^{-6}$ °C^{-1} existed which was consistent across the temperature range.

As-cast and thermally processed composites were studied in a field emission gun (FEG) scanning electron microscope (SEM), JEOL JSM 840F, operating at 3 kV. Microstructural observation was performed on specimens polished using standard metallographic techniques and diamond polishing media. Grain boundaries and second phases in the matrix microstructure were revealed using an etchant of 2% HNO_3 in isopropanol.

Microhardness testing was performed on as-cast and heat-treated 50% V_f composites. Interfibre zones were too small to allow sampling in higher V_f materials. Hardness

measurements were performed on a Vickers scale using a diamond indenter with a 25 g force and a 20 s dwell. Each data point was the mean of at least ten indentations and the error bars represent standard error.

Modelling the thermal strain response of C/Mg

A simple temperature-dependent (matrix flow stress) one-dimensional model for predicting composite axial strain response due to imposed thermal loading has been given by Zhang et al. [8]. The model assumes only the matrix can deform plastically and that the length of the fibre and matrix must remain the same, leading to

$$\varepsilon_{\text{comp}} = \frac{\sigma_{\text{f}}}{E_{\text{f}}} + \alpha_{\text{f}}\Delta T = \frac{\sigma_{\text{m}}}{E_{\text{m}}} + \alpha_{\text{m}}\Delta T + \varepsilon_{\text{m}}^{\text{pl}} \quad (1)$$

where σ and ϵ represent axial stresses and strains; α and E are coefficients of thermal expansion (CTE) and Young's moduli; and ΔT is the change from the reference temperature. Subscripts m, f and comp refer to the matrix, fibre and composite, and pl denotes plastic. Axial force balance dictates that

$$V_{\text{m}}\sigma_{\text{m}} = -V_{\text{f}}\sigma_{\text{f}} \quad (2)$$

where V denotes volume fraction. Combining Eqs. 1 and 2 enables the composite behaviour to be described during cooling from the production temperature and subsequent thermal cycles mimicking actual service conditions.

Property values for 60% and 50% V_{f} P100S/AZ91D are $E_{\text{m}} = 44.8$ GPa; $E_{\text{f}} = 759$ GPa; $\nu_{\text{m}} = 0.35$; $\nu_{\text{f}} = 0.26$; $\alpha_{\text{m}} = 26.8 \times 10^{-6}$ °C^{-1}; $\alpha_{\text{f}} = -1.48 \times 10^{-6}$ °C^{-1}. The experimentally determined V_{f}s of 58.4% and 47.5% were used in the model. The yield stress of AZ91D increased approximately linearly with decreasing temperature (Fig. 1)—values were determined from the fit to the experimental data shown.

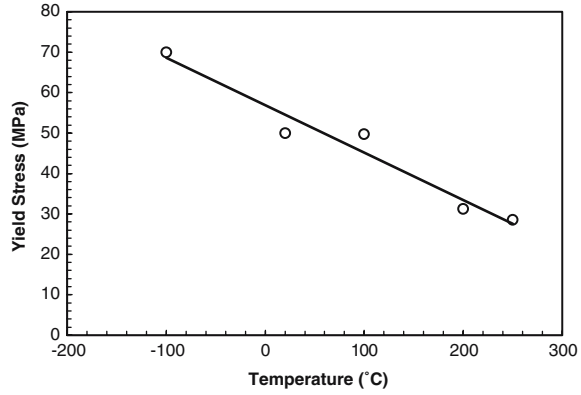

Fig. 1 Plot of yield stress versus temperature for AC AZ91D

In the absence of experimental data the temperature-dependent yield strength values of T6 AZ91D have been assumed to possess the same gradient as the AC AZ91D and shifted to higher strengths to be consistent with a value of 130 MPa at ambient as reported by Caceres et al. [15] for the same alloy, cast using similar techniques and with a comparable grain size (~150 μm). The implications of this strength assumption will be discussed with the analysis results below. The model employed does not account for matrix strain hardening thus no change to the matrix properties arose from cryogenic pre-treatment, only a change in the composite thermal history. All composites are assumed to be stress free at a value of 200 °C during fabrication or during heat treatment.

Results and discussion

Microstructure

The main strengthening phase in AZ91 is the body-centred cubic (*bcc*) $Mg_{17}Al_{12}$ or β phase. β precipitates in three forms: as massive particles on grain boundaries—these being the product of a divorced eutectic reaction from the Al enriched part of the liquid metal that solidifies last during casting; as discontinuous precipitates nucleating at grain boundaries; and as fine continuous precipitates, with plate shaped morphologies, within grains.

As-cast P100S/AZ91D consisted of Mg rich matrix with Al in solid solution and a massive β phase, bridging fibres in areas of higher reinforcement content (Fig. 2a) (arrowed). At grain boundaries and fibre surfaces some lamella discontinuous precipitation of β occurred from the supersaturated solid solution matrix. In addition, continuous β precipitates existed in the α matrix which are too fine to be resolved in the SEM, but which were seen in a TEM investigation not reported here. Continuous and discontinuous precipitates have a defined crystallographic orientation relationship with the matrix (α) i.e. $(0001)_\alpha \parallel (110)_\beta$, $[10\bar{2}1]_\alpha \parallel [1\bar{1}1]_\beta$ where the primary habit plane of β is parallel to the basal plane of the matrix (Burgers relationship) [16, 17].

T6 heat-treating causes partial homogenisation of the microstructure (Fig. 2b). During solution heat treatment most of the β phase was dissolved and the Al placed into solid solution. The 12 h treatment was not sufficiently long to achieve full dissolution of massive $Mg_{17}Al_{12}$. Isolated particles remained at fibre matrix interfaces and grain boundaries after artificial ageing (arrowed), although particle size was reduced significantly. During ageing, discontinuous precipitates formed at high angle grain boundaries and at the fibre matrix interface, and continuous precipitates formed within the grains. It is difficult to distinguish between regions of discontinuous and contin-

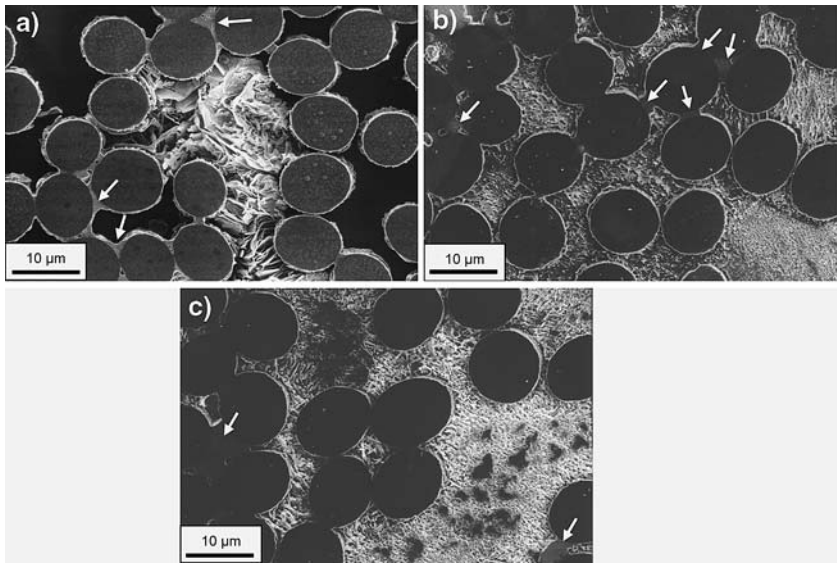

Fig. 2 SEM micrographs of 50% V_f P100S/AZ91D composite in (**a**) AC, (**b**) T6 and (**c**) T6-Cryo condition. Heat-treatment dissolves much of the massive β particles and increases the amount of continuous and discontinuous β precipitates in the matrix

uous precipitation in the etched composites due to the coarseness of the continuous precipitates and the breaking-up and spheroidising of the lamellar discontinuous precipitates during ageing.

No discernible change in the microstructure was observed in cryogenically treated material and these treatments did not induce any cracking or debonding in the specimens examined (Fig. 2c).

Composite thermal expansion behaviour

Figure 3 shows plots of longitudinal thermal strain response of 60% V_f composite between ±100 °C over five thermal cycles. An artefact of the cryogenic control system exists in all dilatometer data herein which is manifested as fluctuations in the strain versus temperature curve during the cooling cycle, at approximately –50 and –80 °C. Several features are apparent from the figure including strain hysteresis and tensile residual plastic strain generation. The large tensile strains generated during the cooling phase of the cycle were not recovered on the return to room temperature and resulted in specimen ratcheting. The amount of residual plastic strain generated during the first cycle is larger than during subsequent cycles. Total strain recorded after five cycles is approximately 410 μm m^{-1}.

Strain hysteresis was also greatest during the first thermal cycle. Little change was observed in the strain hysteresis with progressive cycling after the first cycle. CTE values were both positive and negative over the thermal cycle, ranging from ~0.5×10^{-6} °C^{-1} to -1.3×10^{-6} °C^{-1} the lower value of CTE being close to the fibre CTE of -1.48×10^{-6} °C^{-1}. These low CTE values for the 60% V_f P100S/AZ91D demonstrate the ability to achieve near-zero CTEs in C/Mg composites.

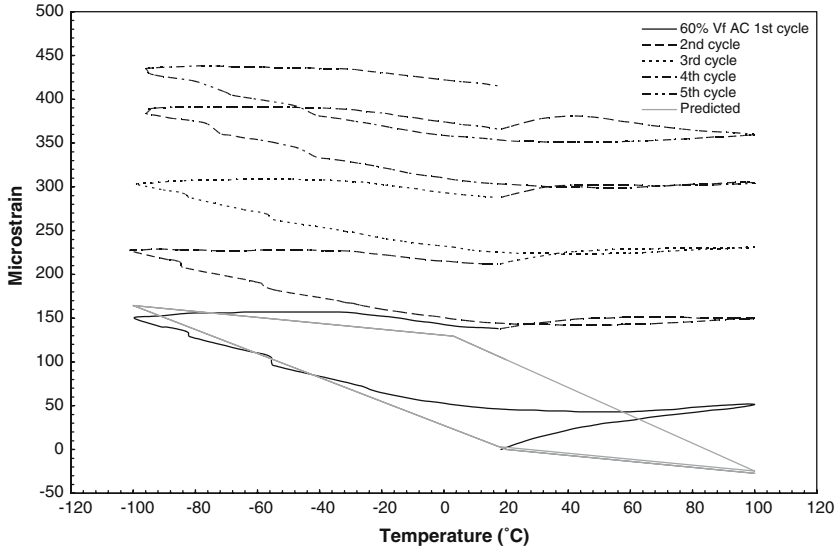

Fig. 3 Thermal strain response of 60% V_f P100S/AZ91D for cycles 1–5 between ±100 °C. —— Cycle 1, – – – cycle 2, ····· cycle 3, –·–· cycle 4, –··– cycle 5 —— simple model prediction

Thermal expansion data for 50% V_f P100S/AZ91D are plotted in Fig. 4. The first cycle behaviour of the composite is markedly different from that of cycles 2–5. As in the higher volume fraction composite, strain hysteresis and residual strain generation were most extreme over the first cycle. Once again residual plastic strain reduces significantly after the first cycle; however, hysteresis remains to a similar extent over the cycles presented. Composite CTE values were encouragingly low and ranged from ~1×10^{-6} °C^{-1} to -0.8×10^{-6} °C^{-1} during the thermal cycle.

The predictions of the strain compatibility model are also shown in Figs. 3 and 4. Due to the positive CTE of AZ91D and the slightly negative CTE of carbon fibres tensile stresses are predicted to build in the matrix on cooling down from production temperatures. The tensile yield point is reached in the matrix before reaching room temperature and further stress generation results in plastic deformation, during which the matrix does not contribute significantly to the composite thermal expansion and fibre properties dominate, so that a portion of negative thermal expansion is predicted. Composites expand elastically with a rule-of-mixtures CTE during the first positive temperature excursion as internal forces are relieved. Upon returning to 20 °C the yield point in tension is reached again and further cooling to –100°C results in large tensile plastic strains in the composite. Reheating first relieves the tensile forces within the matrix elastically and then puts it into compression, again with a rule of mixtures CTE. Once the compressive yield point in the matrix is reached the negative fibre properties are predicted to dominate once more.

Several key differences are apparent between the model's predictions and the experimental results: the results exhibit a more positive CTE (i.e. matrix dominated properties) than the model, especially during heating; after the first thermal cycle the model predicts that the composite expands and contracts about a hysteresis loop with no thermal ratchet. Nevertheless, the model offers a reasonable prediction of the first thermal cycle residual strain and strain hysteresis generation due to the elastic limit of the matrix being exceeded during the thermal cycle.

We suggest that the simple model fails to predict a thermal cycle ratchet due its assumption of perfect interfacial bonding. Madgwick et al. [18] have also suggested that sliding on fibre matrix interfaces is a necessary condition for thermal cycle ratcheting. Sliding has been proposed to occur in two ways, both of which operate to relieve internal stresses generated by differential fibre and matrix strains during the thermal cycle [19]. The first—time-dependent diffusional sliding—occurs at fibre ends, where shear stresses are the largest and is often associated with slow heating/cooling rates and elevated temperatures. The second way for sliding to occur is for the interface to debond during thermal cycling, thus allowing frictional sliding to occur [13, 19].

In the current material the upper temperature (100 °C) is believed to be too low to result in time-dependent sliding [19]. Moreover, previous work by the current authors has shown that P100S/AZ91D exhibits the behaviour of a weakly bonded system and inferred interfacial debonding and frictional sliding through the presence of fibre protrusion after 100 cycles between ±100 °C [20]. Frictional interfacial sliding would be favoured at positive temperatures as the composite cylinder model [21] predicts large compressive radial stresses exist in the matrix at cryogenic temperatures, which will clamp the matrix to the fibre inhibiting sliding. As the composite is heated, clamping stresses will decrease and the fibres will contract in the longitudinal direction while an expansion should occur in

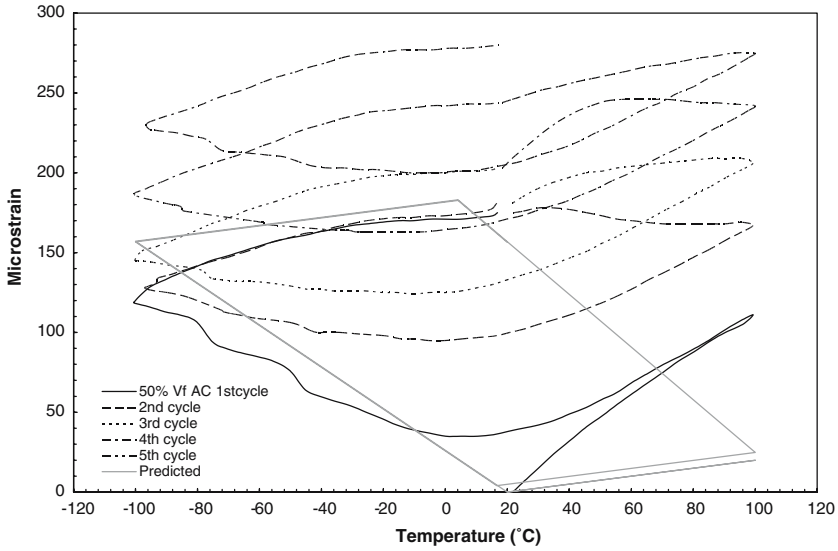

Fig. 4 Thermal strain response of 50% V_f P100S/AZ91D for cycles 1–5 between ±100 °C

the matrix. Interfacial sliding will occur in order to relieve the differential stresses generated in the composite and will cause the matrix to expand away from fibre ends. It is proposed that this expansion is recorded by the dilatometer. The fact that it is caused by the relatively unconstrained matrix explains why it results in a more positive expansion than expected on the basis of the model.

Interfacial sliding may be controlled through tailoring fibre/matrix interfacial bonding which can either be mechanical or chemical in nature, or a combination of the two [22]. In P100S/AZ91D there is little potential for improved mechanical interlocking as fibres are already in the surface treated condition. Therefore, a stronger chemical bond is required, which could be achieved through increased interfacial reaction. The reactivity of fibres cannot be changed due to the requirement for high modulus (lower modulus fibres tend to be more reactive). This means that control of processing parameters, such as preform and melt temperatures [23], to allow increased melt contact times is the only conceivable way of producing a stronger interfacial bond.

Effect of thermal processing on composite thermal expansion behaviour

The non-linear and hysteretic thermal strain response of P100S/AZ91D composites was not eliminated via heat-treating (T6) (Figs. 5, 6), or cryogenically conditioning material in the T6 condition (Figs. 7, 8), regardless of volume fraction. In most cases residual plastic strains still existed after each thermal cycle. A reduction of residual plastic strain during the first thermal cycle was achieved by all material treatments. As a result, materials in the T6-Cryo condition exhibited lower total plastic deformation after five cycles: compare 410 to 270 μm m^{-1} for 60% and 280 to 180 μm m^{-1} for 50% V_f P100S/AZ91D in the AC and T6-Cryo conditions, respectively. However, after the first cycle no material treatment systematically reduced residual strain generation.

The general trend of thermal strain response is remarkably similar in AC or heat-treated P100S/AZ91D composites with a shift in the hysteresis loop to higher strain levels with the progression of thermal cycles and with hysteresis essentially remaining unaffected by thermal cycling.

In both composite V_fs material treatments, regardless of type, resulted in what is an essentially linear material strain response over the initial heating part of the cycle to within experimental accuracy. Large tensile plastic strains occurred in all composites during the cryogenic part of the cycle and showed little response to heat-treatment and conditioning.

As previously indicated the model can be used to assess the composite response during the thermal cycle. In T6 composites, as was the case for the AC material, at the start of thermal cycling the matrix is in a plastic tensile state. Furthermore, heating is purely an elastic event and cooling past room temperature renters the tensile plastic zone. At this point, due to the projected increase in strength, upon heating and subsequent cycling the matrix is predicted to operate elastically as the change in temperature is not sufficient to relieve the tensile stress and surpass the compressive yield point.

Cryogenic treatment alters the thermal history of the composite, placing the matrix in a tensile plastic state so that the return to ambient does not induce compressive yielding. Therefore, at the start of thermal cycling the matrix yield point is soon reached (~40 °C, Figs. 7, 8) and induces plastic strain generation with a negative CTE. Now due to the increase in strength the cooling to –100 °C does

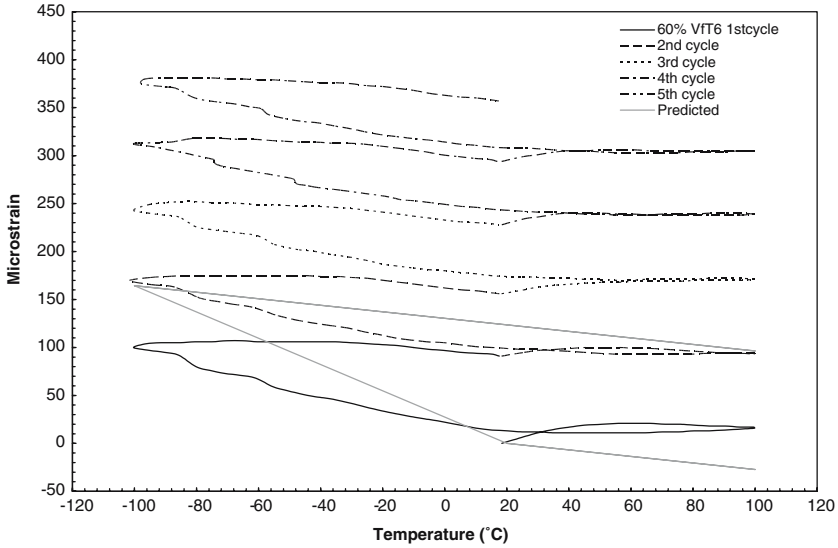

Fig. 5 Thermal strain response of T6 heat-treated 60% V_f P100S/AZ91D composite for cycles 1–5 between ±100 °C

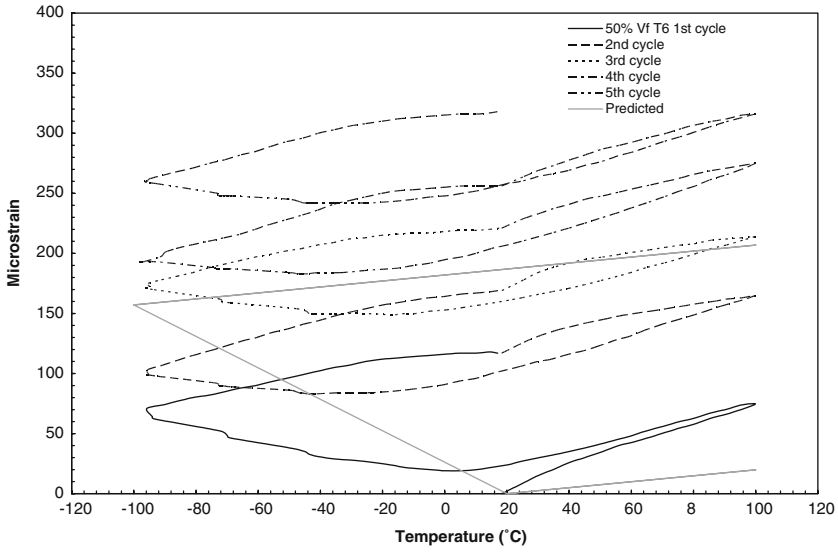

Fig. 6 Thermal strain response of T6 heat-treated 50% V_f P100S/AZ91D composite for cycles 1–5 between ±100 °C

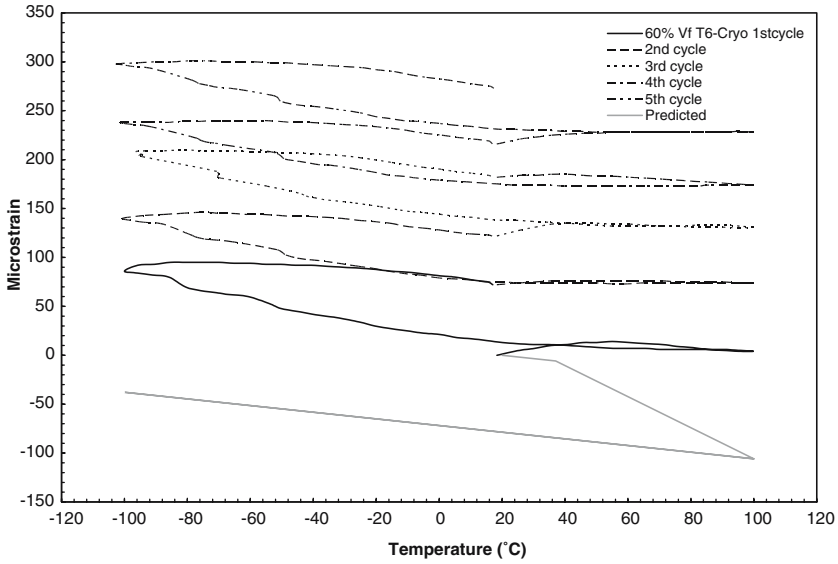

Fig. 7 Thermal strain response of 60% V_f P100S/AZ91D composite in the T6-Cryo condition for cycles 1–5 between ±100 °C

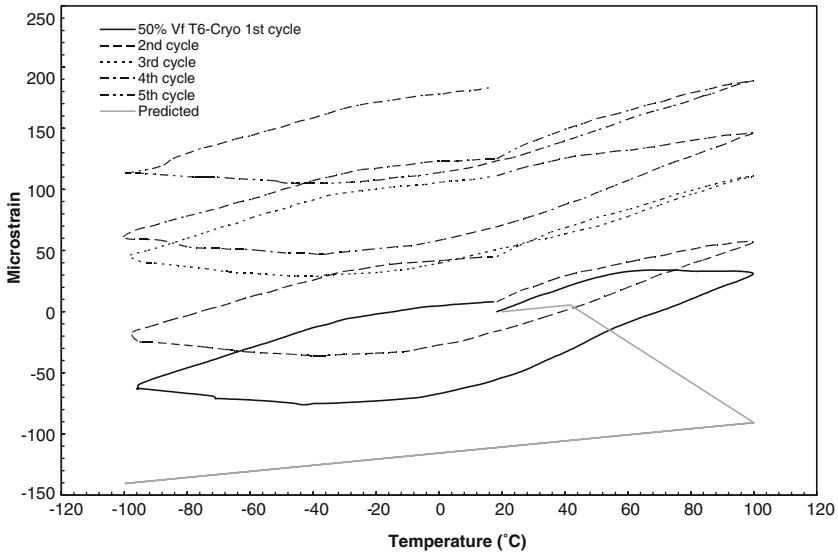

Fig. 8 Thermal strain response of 50% V_f P100S/AZ91D composite in the T6-Cryo condition for cycles 1–5 between ±100 °C

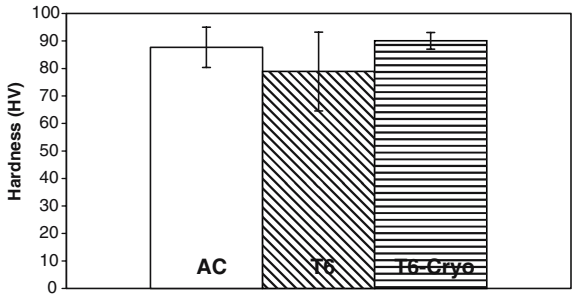

Fig. 9 Plot showing matrix microhardness as a function of thermal treatment

not result in sufficient compressive stress relief and tensile stress generation to exceed yield, thus once again the cycle is predicted to enter a stable elastic regime.

Model predictions suggest after an initial instability T6 and T6-cryo treated composite materials could behave in a linear manner over the temperature cycle. Contrary to this during experiments the elastic limit of the matrix is clearly exceeded during cycling (hysteresis loops). This suggests the matrix yield strength value has been assumed to be too high in the model or there is a Bauschinger effect in that reverse cycling induces matrix plasticity after smaller temperature changes.

The fact that the matrix yield strength has been little affected by heat-treatment is supported by matrix microhardness measurements (Fig. 9). The principal strengthening mechanism in Mg–Al alloys is considered to be the obstruction of basal glide and therefore, encouragement of cross-slip, through continuous β precipitation [16]. Thus, artificial aging after solution treating is recognised to maximise the yield strength of Mg–Al alloys at the expense of some ductility and toughness [17]. However, the coarseness of the continuous β-precipitates in T6 P100S/AZ91D as shown in Fig. 2b and c probably prevents them from being efficient obstacles to dislocation motion, thereby reducing the extent of any yield strength increase.

Once again, plastic residual strain generation indicates that interfacial sliding occurs. Therefore, it can be concluded that the T6 heat-treatment does not alter the interfacial bond to make it more resistant to interfacial debonding.

In a satellite application observable strain hysteresis and thermal strain ratcheting in P100S/AZ91D may result in unwanted structural deformation. A C/Mg composite with a linear thermal response over the temperature cycle may therefore represent an improvement over the current materials provided a low CTE can be maintained. Thermal strain generation could be minimised by limiting the change in temperature experienced by the system. However, if this is not possible then a linear thermal strain response may still be achievable provided that the matrix yield strength can be increased sufficiently so that it is not exceeded during the cycle. The prevention of interfacial sliding is also required.

Further scope may exist for improving the yield strength of AZ91 through grain refinement [15] and stabilisation of the β phase via calcium and rare earth additions [24], although Ca additions are probably not suitable as they have a tendency to reduce the axial strength of C/Mg composites due to the formation of brittle Mg_2Ca phases [25]. Higher strength Mg-alloys are available such as copper (Mg–Cu) or nickel (Mg–Ni) particulate reinforced composites [26, 27]; and the more commercial rare earth (RE) containing WE54, WE45 and QE22 alloys. The RE alloys possess yield strengths of ~200 MPa with improved creep resistance, but not without a cost penalty [28] and the potential for detrimental interfacial reactions as large (~0.1 μm) rare earth (cerium and lanthanum) oxides can lead to embrittlement of C/Mg composites [29]. Despite their superior strengths the benefit of Mg–Ni alloys would perhaps be offset by the formation of brittle Ni/Mg compounds which were associated with premature fibre failure in a C/Mg composite with Ni-coated fibres [30]. Mg–Cu would be suited because Cu and C are unreactive [31]. Furthermore Cu additions could be introduced to improve the properties of AZ91 as shown by Hassan et al. [32]. However, it is doubtful the disintegrated melt deposition process for Mg–Cu and Mg–Ni alloy production could be extended for continuous fibre composite production.

Conclusions

- UD P100S/AZ91D composites exhibited complex non-linear and hysteretic thermal expansion behaviours over the ±100 °C temperature range.
- The thermal strain response of UHM C/Mg composites can be predicted to reasonable accuracy using the simple 1D model, especially during the first thermal cycle. Future models must incorporate frictional sliding in the analysis to provide accurate predictions of the thermal expansion behaviour of weakly bonded composite systems.
- Interfacial sliding must have occurred in the C/Mg specimens for thermal strain ratcheting to occur as perfectly bonded samples were predicted to behave in a hysteretic manner with no thermal ratchet.
- The non-linear and hysteretic thermal strain response of P100S/AZ91D was not eliminated by heat-treating or cryogenically conditioning the material (in T6 condition) regardless of volume fraction.
- The similarity between thermal expansion behaviour in AC/T6/T6-Cryo composites (albeit with slightly lower

first cycle ratchets) would suggest that only material thermal history is affected and not the matrix yield strength. This is supported by matrix micro-hardness data and was suggested to be due to the coarse distribution of β in the heat-treated matrix microstructure.

Acknowledgements The authors wish to thank P. Allen, Hexcel Composites, Duxford, England for kindly allowing the use of the Linseis cryogenic dilatometer and J. Reiter (LKR) for the fabrication of C/Mg specimens. Thanks are also due to P. Schulz (LKR) for his valuable discussions.

References

1. Maclean BJ, Misra MS (1982) In: Proc Symp Mechanical Behaviour of Metal Matrix Composites. AIME, Dallas, TX, pp 195–212
2. Wolff EG, Kendall EG, Riley WC (1980) In: Proc 3rd Int Conf Comp Mater Paris 26–29 August. Pergamon Press, pp 1140–1152
3. Badini C, Ferraris M, Marchetti F (1994) Mater Lett 21(1):55
4. Wolff EG, Min BK, Kural MH (1985) J Mater Sci 20(4):1141
5. Kural MH, Min BK (1984) J Comp Mater 18(6):519
6. Min BK, Crossman FW (1981) In: Hahn TA (ed) Proc 8th Int Thermal Expansion Symp. National Bureau of Standards, Gaithersburg, Maryland; Plenum, New York, pp 175–188, June 1981
7. Kiehn J, Bohm E, Kainer KU (1997) In: Proc 1st Int Conf Ceramic and Metal Matrix Composites, vol 127. pp 861–867
8. Zhang HY, Anderson PM, Daehn GS (1994) Metall Trans A 25(2):415
9. Armstrong JH, Rawal SP, Misra MS (1990) Mater Sci Eng A 126:119
10. Tsai S-D, Mahulikap D, Marcus HL, Noyan IC, Cohen JB (1981) Mater Sci Eng 47:145
11. Tompkins SS (1989) In: Johnson WS (ed) Metal matrix composites: testing, analysis, and failure modes – ASTM STP 1032. ASTM, Philadelphia, pp 54–67
12. Tompkins SS, Sharpe GR (1986) In: Proc 18th Int SAMPE Technical Conf. SAMPE, pp 623–637
13. Mitra S, Dutta I, Hansen RC (1991) J Mater Sci 26(22):6223
14. Diwanji AP, Hall IW (1992) J Mater Sci 27(8):2093
15. Caceres CH, Davidson CJ, Griffiths JR, Newton CL (2002) Mater Sci Eng A 325(1–2):344
16. Clarke JB (1968) Acta Metall Mater 16:141
17. Celotto S (2000) Acta Mater 48(8):1775
18. Madgwick A, Mori T, Withers PJ, Wakashima K (2001) Mech Mater 33:493
19. Dutta I (2000) Acta Mater 48(5):1055
20. Russell-Stevens M, Todd RI, Papakyriacou M (2005) Mater Sci Eng A 397(1–2):249
21. Vedula M, Pangborn RN, Queeney RA (1988) Composites 19(2):133
22. Feldhoff A, Pippel E, Woltersdorf J (1997) J Microsc 185:122
23. Capel H, Harris SJ, Schulz P, Kaufmann H (2000) Mater Sci Technol 16(7–8):765
24. Wenwen D, Yangshan S, Xuegang M, Feng X, Min Z, Dengyun W (2003) Mater Sci Eng A356:1
25. Beffort O, Hausmann C (2000) Magnesium alloys and their applications. Wiley-VCH, Munich, Germany, pp 215
26. Hassan SF, Gupta M (2003) Mater Sci Technol 19(2):253
27. Hassan SF, Gupta M (2002) J Mater Sci 37(12):2467
28. Polmear IJ (1981) Light alloys—metallurgy of the light alloys. Edward Arnold, London
29. Chin ESC, Nunes J (1987) J Met 39(10):A32
30. Hall IW (1987) Metallography 20(2):237
31. Lin MH, Buchgraber W, Korb G, Kao PW (2002) Scr Mater 46:169
32. Hassan SF, Ho KF, Gupta M (2004) Mater Lett 58(16):2143